V2O5 as an inexpensive counter electrode for dye sensitized solar cells

V_2O_5 as an inexpensive counter electrode for dye sensitized solar cells

Geeta R. Mutta[1*], Srinivasa R. Popuri[2], Michal Maciejczyk[3], Neil Robertson[3], M. Vasundhara[4]
John I. B. Wilson[5], Nick S. Bennett[1]

[1]Nano-Materials Laboratory, IMPEE-EPS, Heriot Watt University, Edinburgh EH14 4AS, United Kingdom

[2]Centre for Advanced Energy Storage and Recovery, ICS-EPS, Heriot Watt University, Edinburgh EH14 4AS, United Kingdom

[3]School of Chemistry and EaStCHEM, University of Edinburgh, Edinburgh, EH9 3FJ, United Kingdom

[4]Materials Science and Technology Division, CSIR-National Institute for Interdisciplinary Science and Technology, Industrial Estate, Trivandrum 695019, India

[5]Institute of Photonics and Quantum Sciences, IPAQS-EPS, Heriot Watt University, United Kingdom

*Corresponding author: geeta.mutta@gmail.com

Abstract

In pursuit of an abundant, inexpensive and stable counter electrode as an alternative to platinum for dye-sensitized solar cells (DSSCs), we report a new, low-cost substitute material. Here for the first time, we demonstrate that V_2O_5 can be used as a counter electrode material in DSSCs. We note that the efficiency of DSSCs with commercial V_2O_5 and hydrothermal treated V_2O_5 are upto 1.2% and 1.6%, respectively. The results indicate that, with optimization, V_2O_5 can be a promising choice to replace platinum from a cost perspective. The innovation of new economical counter electrodes offers a potential way to cut down the industrial costs which is crucial for large-scale production and commercial applications of DSSCs.

1. Introduction

Global warming is a major concern of today's world. Hence, there is an urgent need for environmentally sustainable energy technologies. Solar energy is the source of an enormous quantity of clean, renewable energy; it has attracted much attention as photovoltaic (PV) cells can directly convert solar energy into electrical energy with low carbon footprint. Despite being an abundant source of energy and promising industry, only approximately 0.015% of global electricity is generated from solar energy, however this could be massively extended by further reductions in cost and development of new markets for PV. In this context, dye sensitized solar cells (DSSCs) have emerged as an interesting low-cost photovoltaic technology [1]. Furthermore, the other key attributes of DSSC technology are its simple manufacturing procedures, environmental friendliness, light-weight, flexibility, semi transparency and good performance in diverse light conditions [2].

DSSCs have stimulated great research interest since the first report of high-efficiency from O'Regan and Grätzel in 1991 [1]. Although laboratory device efficiencies have reached 12% [3], to make this available for mass production, the cost of manufacture has to be reduced. DSSCs mainly consist of a photoanode, made of a few micron thick semiconductor such as TiO_2 on a conductive substrate such as fluorine doped tin oxide coated glass (FTO), an organic sensitizer (dye, e.g. N719) or inorganic sensitizer (quantum dots, e.g. CdS, PbS), an electrolyte (typically I_3^-/I^- or Co^{2+}/Co^{3+} redox couples) and a counter electrode (CE) made of platinum (Pt) or a carbon material on a conductive substrate. Each component of the device decides the efficiency and cost of the resulting solar cell. In order to achieve economic viability, one of the challenges in DSSC technology is to find a suitable replacement for the precious metal Pt. Pt is a preferred CE because of its excellent electrocatalytic activity and high electrical conductivity [4]. There are some reports which claim that Pt reacts with I_3^- in the electrolyte to form PtI_4 [5] and in

addition the catalytic activity decreases upon the exposure to dye solution and in the presence of I_2 based electrolyte [6]. Additionally, Pt is a rare and expensive metal. To reduce the fabrication cost, substantial research efforts have been placed on the exploration of alternative and cheap counter electrodes. To date carbon materials [7, 8, 9, 10], conductive polymers [11, 12, 13], inorganic compounds such as sulfides [14, 15, 16], carbides [17], nitrides [18, 19], phosphides [20], tellurides [21], and composites [22, 23, 24] have been explored as effective alternative counter electrodes. Though some of these materials have reached the efficiencies comparable to or slightly inferior to that of existing Pt, there still remain concerns of ready availability, eco-friendliness, stability, economical viability and large scale production cost. Therefore, the fact remains that very few alternative materials are capable of replacing the expensive Pt in fabricating economical and highly efficient DSSCs. Despite having a number of strengths such as durability, environmental friendliness, stability, high melting temperatures, and high electrical and thermal conductivities, oxides [25, 26] are less studied compared to other inorganic materials. Recently tungsten oxide [26, 27] has been reported as an efficient low cost CE.

Vanadium based oxides belongs to transitional metal oxides which are of particular interest because of their low cost, abundance in nature, good electrical conductivities, good catalytic activity and excellent atmospheric stability. It is known that V_2O_5 is already considered as a promising material in technologies as cathodes in rechargeable ion batteries [28], optical electrical switches [29], spintronic devices [30], gas detectors [31], capacitors [32], and electro-chromic devices [33]. In this present work, we choose V_2O_5 as a material of interest for counter electrodes in DSSCs, because of its distinctive features: inexpensive, readily available, has excellent physical and chemical properties, and reasonable electrical conductivity. There are a few reports on the implementation of V_2O_5 in DSSC technology such as an electron blocking

layer [34] or a compact layer [35], and a composite of V_2O_5 in solid state DSSCs [36, 37]. To the best of our knowledge, this is the first time ever that V_2O_5 to be used as a CE in DSSCs. In this report, we show that the photovoltaic performance of hydrothermally treated V_2O_5 (H-V_2O_5) shows better photoconversion efficiency compared to commercial V_2O_5 (C-V_2O_5) and has the potential to compete with expensive Pt counter electrodes. It is worthwhile to mention here that, the adhesion issues associated with C-V_2O_5 during film process prompted us to treat this material hydrothermally to alter its particle sizes and improve the film process. So proper care has been taken in terms of hydrothermal synthesis conditions (temperature and duration) to avoid formation of any kind of hydrate or mixed valent vanadium oxide phases.

2. Experimental

2.1. Materials synthesis

Sigma Aldrich analytical grade V_2O_5 powder was used as-received without further purification. An aqueous solution of vanadium oxide was prepared by dissolving C-V_2O_5 in double distilled water under magnetic stirring. After complete dissolution, the resulting solution was transferred to a teflon-lined stainless steel autoclave of 30 mL volume for thermal treatment at 180^{o}C. Once the reaction time was complete, the autoclaves were cooled down to ambient temperature naturally; the resultant yellow powders were collected and rinsed with distilled water and then with ethanol several times; the final products (H-V_2O_5) were finally dried in an oven at 50^{o}C for 6 hours and used for further characterizations.

2.2. Preparation of TiO_2 working electrode

FTO glass substrates (Pilkington TEC glass™, sheet resistance: 11.7 Ω/sq, 2.2 mm in thickness, TEC-12) were cut into small pieces (2 × 2 cm). The substrates were first cleaned thoroughly

with soapy water, and then ultrasonicated in deionised water followed by acetone and iso-propanol for 15 min at each step, and then dried in flowing nitrogen to further remove any solvent traces. After drying, the substrates were treated with 40 mM $TiCl_4$ for 1 hour at 80°C to prepare a compact layer of TiO_2. Commercially available TiO_2 pastes (DSL 18NR-T, Dyesol as the transparent layer and DSL 18NR-AO, Dyesol as the scattering layer) were screen printed on the compact layered FTO substrates whose active areas were approximately 1 cm^2. The TiO_2 coated films were then successively heated in ambient air on a hotplate at 325°C for 10 min, at 375°C for 5 min, at 450°C for 15 min and at 500°C for 15 min, before being cooled down slowly to room temperature. Afterwards these electrodes were further treated with 40 mM $TiCl_4$ for 30 min at 80°C followed by sintering at 450°C for 30 min. As soon as the working electrodes (WE) reach 80°C, these films were subsequently immersed in N719 (Dyesol) solution and kept in an air-tight glass container at room temperature under dark and dry conditions for a day. Dye sensitized photoanodes were washed with iso-propanol to remove the excess dye which was firmly attached to the surfaces of TiO_2, followed by drying with nitrogen flow at room temperature.

2.3. Preparation of counter electrodes

FTO coated glass was cut into the same dimensions as the WE and a small hole was drilled to facilitate the injection of electrolyte, using a sand blasting unit, with a smooth finish given by ending the drilling with a portable glass hole drilling tool. The drilled FTO substrates were subjected to the same cleaning and drying procedures as was the case for the photoanode substrates. C-V_2O_5 and H-V_2O_5 pastes were prepared by mixing 4:1 ratio of V_2O_5 powders with ethyl cellulose and few drops of α-terpineol to make an appropriate viscous paste to facilitate the screen printing process. Finally the V_2O_5 films were prepared by screen printing on the as-

prepared FTO substrates followed by sintering in air at 450°C for 30 min at a heating rate of 5°C/min to remove the binders. Then the V_2O_5 films were allowed to cool down to room temperature. For comparison, a Pt CE was prepared using a sputtering system on FTO substrates. Three kinds of DSSCs were therefore fabricated, i.e. using Pt, C-V_2O_5 and H-V_2O_5 as counter electrodes, and their performances were compared.

2.4. Fabrication of photovoltaic cells

The dye sensitized TiO_2 photoanodes and counter electrodes (sputtered Pt, V_2O_5 screen printed) were assembled into a sandwich configuration with a 25 μm hot-melt spacer (SX1170-60, Solaronix) through the hot-press method by heating at 120°C for few seconds. After assembling the cells, the electrolyte solution (composed of 0.6 M 1-butyl-3-methylimidazolium iodide, 0.05 M iodine, 0.1 M lithium iodine and 0.5 M 4-tert-butylpyridine in acetonitrile) was then injected into the space between the WE and CE via a hole in the CE by capillary effect under vacuum. The hole was then sealed with cover-glass using surlyn. The effective cell area was 1 cm^2. A lead based alloy was ultrasonically soldered for contacts at the edge of the electrodes to make a good current collector. Five cells were prepared for each material.

2.5. Characterization of counter electrodes and DSSCs

The phase purity and crystallographic structure of commercial and as-synthesized V_2O_5 was determined using automated PANalytical X' Pert Diffractometer, Netherlands (using Ni filtered Cu K_α radiation, λ= 1.5406 Å). The diffraction patterns were recorded in the range of 10°-80°. Lattice parameters were extracted from XRD patterns at room temperature using FullProf program suite [38]. The surface morphology of C-V_2O_5 and H-V_2O_5 powder samples and also the counter electrodes were investigated by field emission scanning electron microscopy (SEM) (Quanta 650 FEG ESEM). The optical absorption of commercial and hydrothermal treated

powder samples were measured by diffuse reflectance at room temperature using a Perkin Elmer Lambda 950 UV-VIS-NIR spectrophotometer. Cyclic voltammetry measurements were performed at room temperature using a μAUTOLAB Type III Potentiostat set-up which was driven by the electrochemical software GPES.The photocurrent density and voltage characteristics of DSSCs were measured by computer-controlled digital source meter (Keithley 2400) under AM 1.5 one-sun illumination using a solar simulator (92250 A, Newport, USA). All the fabricated cells were tested at a light intensity of 100 $W\text{-}m^{-2}$ with an active cell area of 0.25 cm^2, which was defined by a mask. An electrochemical work station system (Autolab potentiostat equipped with FRA2 module) was employed to measure the internal resistances of the cells. The impedance spectra were collected under dark conditions by varying the frequency from 0.1 Hz to 1 MHz at an AC amplitude of 10 mV.

3. Results and discussion

3.1. Structure, morphology and optical properties of V_2O_5

3.1.1. X-ray diffraction

The crystallographic structures of C-V_2O_5 and H-V_2O_5 were investigated by X-ray diffraction (XRD). Figure 1 shows the XRD patterns of C-V_2O_5 and V_2O_5 after hydrothermal reaction at 180^oC. All the observed XRD reflections are well indexed to standard JCPDS pattern: #89-0612. Although the overall XRD pattern of the sample that underwent hydrothermal reaction exhibits no obvious difference when compared with that of the C-V_2O_5, the relative intensities of XRD reflections are diminished by approximately 3 times. This indicates a decrease of the crystallinity and particle size of the V_2O_5 sample after hydrothermal reaction. Furthermore, no other peaks of impurities were observed, indicating that phase was retained under hydrothermal conditions.

Using LeBail profile matching analysis, XRD data are indexed with orthorhombic crystal system with space group P m m n and lattice parameters are calculated as a=11.5114(5) Å, b=3.5634(2) Å, c=4.3717(2) Å and unit cell volume V=179.33(2) $Å^3$. The slight changes in the lattice parameters compared to standard JCPDS data could be due to changes in the crystallite size and corroborated with the subsequent morphological studies. The comparatively lower intensity of the H-V_2O_5 sample in XRD results is ascribed to a reduction of particle size. The crystal domain size of the C-V_2O_5 and H-V_2O_5 particles estimated from the Debye-Scherrer formula are 760 nm and 340 nm respectively and this further suggests changes in the crystal size after hydrothermal treatment, which is additionally confirmed in the following SEM micrographs.

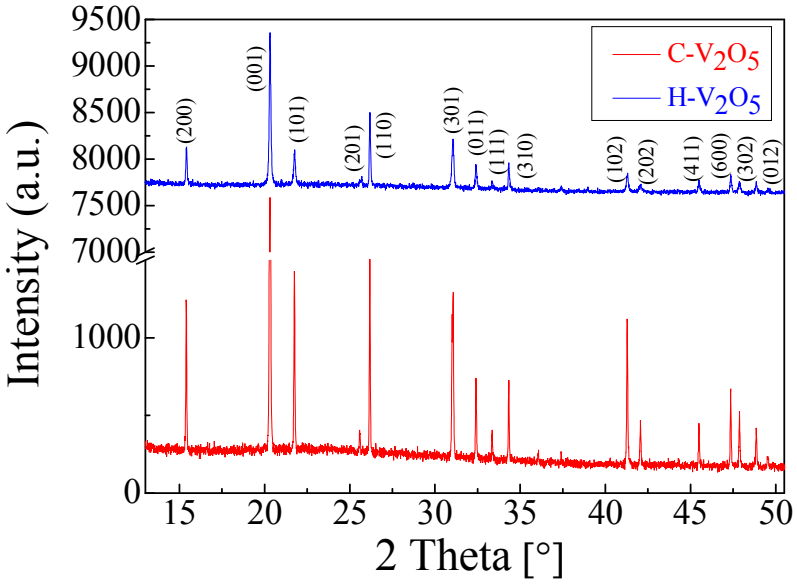

Figure 1. Powder XRD patterns of C-V_2O_5 and H-V_2O_5.

3.1.2. Morphological study by FESEM

Figure 2 shows the surface morphologies of C-V_2O_5, H-V_2O_5 powders and counter electrodes made of these materials studied using FESEM. For direct comparison of commercial, hydrothermal treated powder samples, and their corresponding counter electrodes, the SEM

micrographs were taken with the same conditions and magnification. Figure 2(a) presents the surface morphology of C-V_2O_5 consisted of agglomerated particles that were fused to each other with a non-uniform size which falls in the range of 1 µm - 50 µm. The hydrothermal treatment to the commercial bulk V_2O_5 facilitated to reduce the agglomeration of particles and transformed into a rod like structures as shown in figure 2(b) whose size ranging from a few nm - 1 µm. The C-V_2O_5 counter electrodes shown in figure 2(c) presence of some visible large clusters of several micrometres. Figure 2(d) displays the surface morphology of H-V_2O_5 counter electrodes which is more homogeneous and consists of micro-rod like structures of diameter ~100 nm. This is possibly due to less adhesion taking place between the C-V_2O_5 powder and the FTO substrate, which thus produces more granular features compared to that of H-V_2O_5 films.

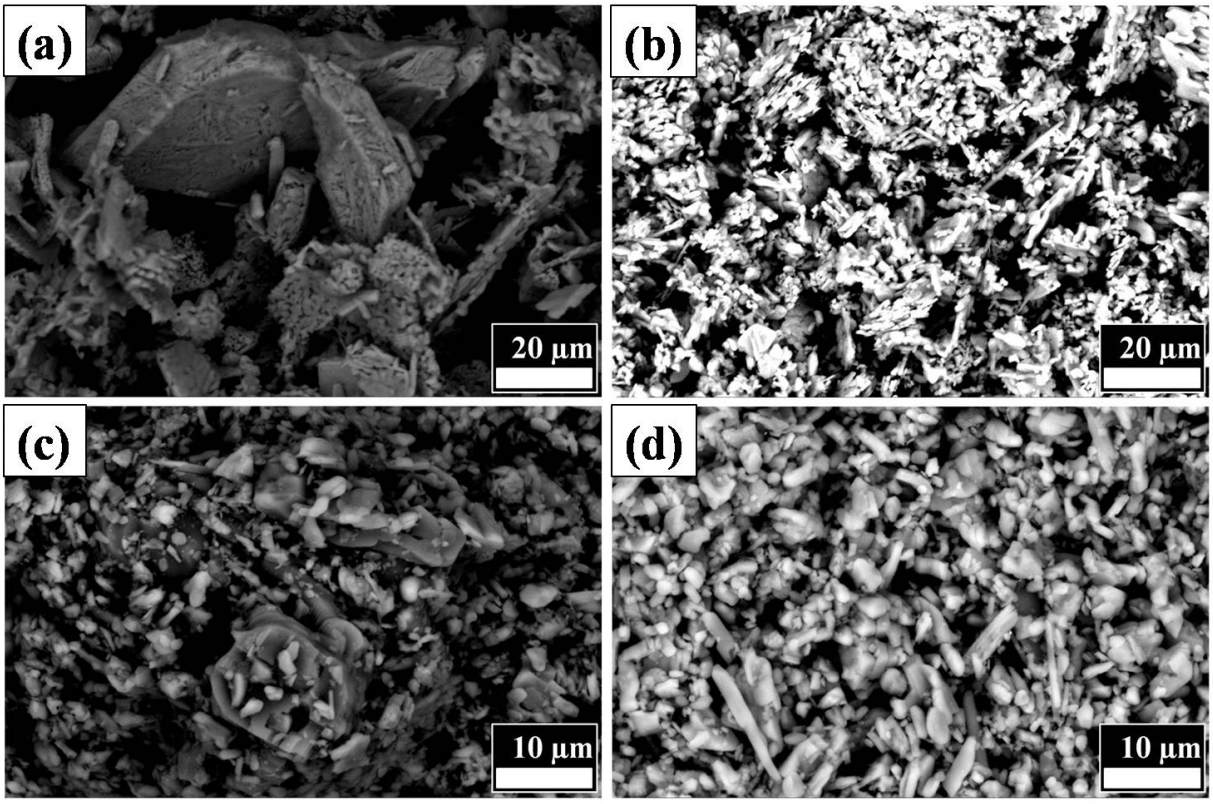

Figure 2. SEM images of (a) C-V_2O_5 powder, (b) H-V_2O_5 powder, (c) C-V_2O_5 made CE and (d) H- V_2O_5 made CE.

From the SEM analysis, we can conclude that the H-V_2O_5 film appears to be smoother than that of the commercial one and its effect expected to reflect in the photovoltaic properties.

3.1.3. Optical absorption spectra

UV-Vis-NIR spectroscopy is a useful technique to measure the optical band gap. The UV-Vis absorption measurements were carried at room temperature in diffuse reflectance mode in the wavelength range 350 nm - 800 nm. The reflectance of the films prepared on glass substrates were measured by subtracting the reflectance of glass substrate as a reference. Figure 3(a) shows the reflectance spectra of commercial and as prepared V_2O_5 powders. It is observed that both the specimens show a strong absorption around 495 nm - 570 nm. The absorption coefficient of both the specimens is calculated from their reflectance spectra by means of following relation.

$$2\alpha t = ln\left(\frac{R_{max}-R_{min}}{R-R_{min}}\right) \quad (1)$$

where the reflectance falls between R_{max} and R_{min} due to absorption by the material and R is the reflectance of any intermediate energy photons. The optical band gap energy of a material can be determined by using the Tauc relation [39], shown below,

$$\alpha h\nu = A\left(h\nu - \mathrm{E_g}\right)^n \quad (2)$$

where $h\nu$ is the incident photon energy, A is a constant and $\mathrm{E_g}$ is the optical band gap of the material and n depends on the type of transition. n=1/2, 2, 3 and 3/2 correspond to allowed direct, allowed indirect, forbidden direct and forbidden indirect transitions, respectively. The direct optical band gap of the material can be determined by plotting $(\alpha h\nu)^2$ versus $h\nu$ as shown in figure 3(b), and then extrapolating the linear portion of the curve to the energy axis for zero absorption coefficients. The direct band gap of H-V_2O_5 is found to be around 2.19 eV,

which is higher than that of C-V_2O_5 value 2.13 eV. The slight increase in band gap of hydrothermal treated powder compared to the commercial one can be ascribed to the decrease of crystallite size, as confirmed from XRD and SEM measurements.

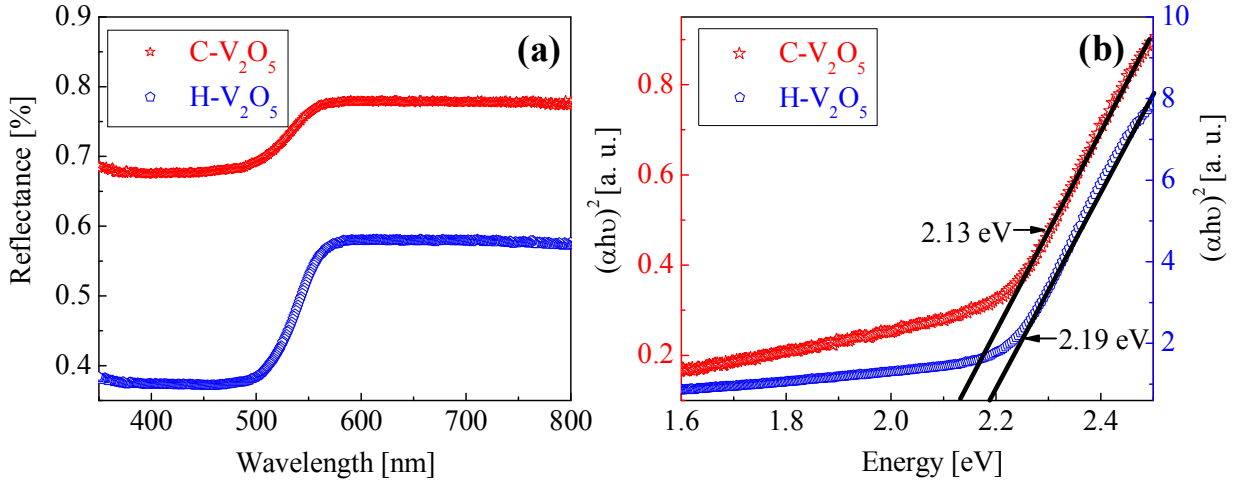

Figure 3. (a) Reflectance vs. wavelength plot of commercial and as prepared V_2O_5 powders. (b) Plot to estimate the direct optical band gap of C-V_2O_5 and H-V_2O_5 powder materials.

3.2 Cyclic voltammetry studies

One of the key parameters in a DSSC is the electrocatalytic activity of the CE and it is well known that cyclic voltammetry (CV) measurements are an essential electrochemical characterization tool to elucidate the interfacial charge transfer properties of the liquid electrolyte on the electrode surfaces. The CV scans were recorded at a scan rate of 20 mV-s^{-1} in a three electrode system in a freshly prepared acetonitrile solution containing 0.1 M lithium perchlorate, 10 mM lithium iodine and 1 mM iodine, which was purged with nitrogen prior to each measurement. The three electrode system comprised of Ag/AgCl as the reference electrode (RE), Pt wire as the (CE) and Pt-coated or V_2O_5 screen printed FTO glass as a WE. Peak to peak separation (EPP) is an important parameter, which qualifies the catalytic activity of CEs. Figure 4 shows the CV curves of the tri-iodide/iodide redox couple for Pt, C-V_2O_5, and H-V_2O_5

electrodes, respectively. Two distinct pairs of redox peaks were obtained in cyclic voltammograms for the Pt CE, indicating its high catalytic activity. The lower potential redox pair can be attributed to reaction 1 (below) whereas the higher potential pair can be represented by reaction 2:

$$\text{Reaction 1:} \quad I_3^- + 2e^- = 3\text{I}^- \tag{3}$$

$$\text{Reaction 2:} \quad 3I_2 + 2e^- = 2I_3^- \tag{4}$$

From the EPPs of the Pt CE and the V_2O_5 counter electrodes, it is clear that the sputtered Pt is catalytically more active towards the reduction of I_3^- to I^- however, the commercial and hydrothermal treated V_2O_5 counter electrodes also show reasonable catalytic activity. It is to be noted that our visual observations by naked eye did not see any peeling off V_2O_5 from FTO substrate after cyclic voltammetry measurements which show the adhesion of V_2O_5 was reasonable.

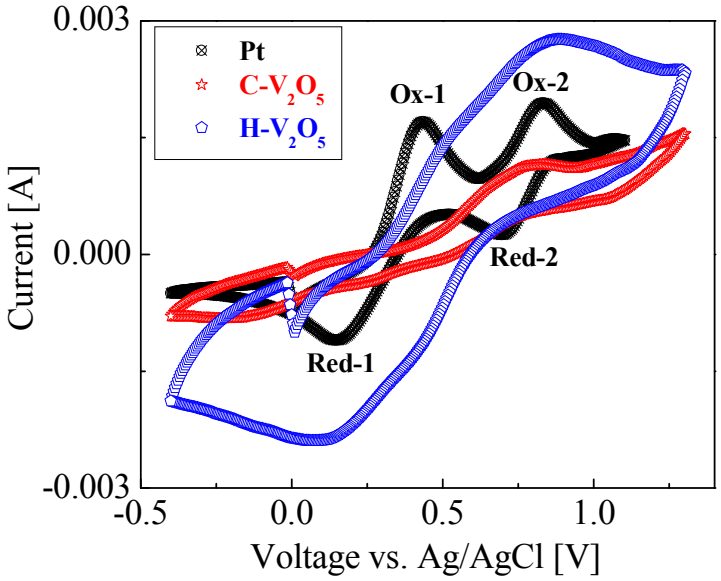

Figure 4. Cyclic voltammogram of iodide/tri-iodide redox species for C-V_2O_5, H-V_2O_5 and Pt counter electrodes.

3.3. Photovoltaic characteristics

The photovoltaic performance of assembled DSSCs based on C-V_2O_5, H-V_2O_5 and Pt counter electrodes are described under illumination conditions of AM 1.5 G (100 mW-cm^{-2}) with an active cell area of 0.25 cm^2. The photoconversion efficiency (η) and fill factor (FF) of the DSSCs are obtained from J-V curves, which were calculated according to the relations:

$$\eta = \left(\frac{V_{oc} \times J_{sc} \times FF}{P_{in}}\right) \times 100 \quad (5)$$

$$FF = \left(\frac{V_{max} \times J_{max}}{V_{oc} \times J_{sc}}\right) \quad (6)$$

where V_{max} and J_{max} are voltage and current density for the maximum power output, V_{oc} is the open-circuit voltage, J_{sc} is the short-circuit current density and P_{in} is the incident light power. Figure 5 displays the comparison of DSSC performance of C-V_2O_5, H-V_2O_5 and Pt counter electrodes and their photovoltaic characteristics are also summarized in Table 1. The efficiency of the cell with Pt CE is 6.9%. The champion cells made of C-V_2O_5 and H-V_2O_5 counter electrodes exhibits the maximum efficiencies of 1.2% and 1.6% respectively. J_{sc} for the device based on H-V_2O_5 CE is higher than that of C-V_2O_5, suggesting that the H-V_2O_5 based CE has better surface area (as seen in SEM micrographs in figure 2(c) and figure 2(d)), which has enhanced the electrochemical performance.

Both C-V_2O_5, and H-V_2O_5 cells have increased series resistance (R_s) compared with the reference cell, and also have lower shunt resistances (R_{sh}), all of which reduce the FFs to 29% and 27% respectively. The lower series resistance in case of H-V_2O_5 compared with C-V_2O_5, indicates the better adhesion of the material to the FTO substrate. It is clear that the J-V properties of the devices are sensitive to surface morphology of the CE.

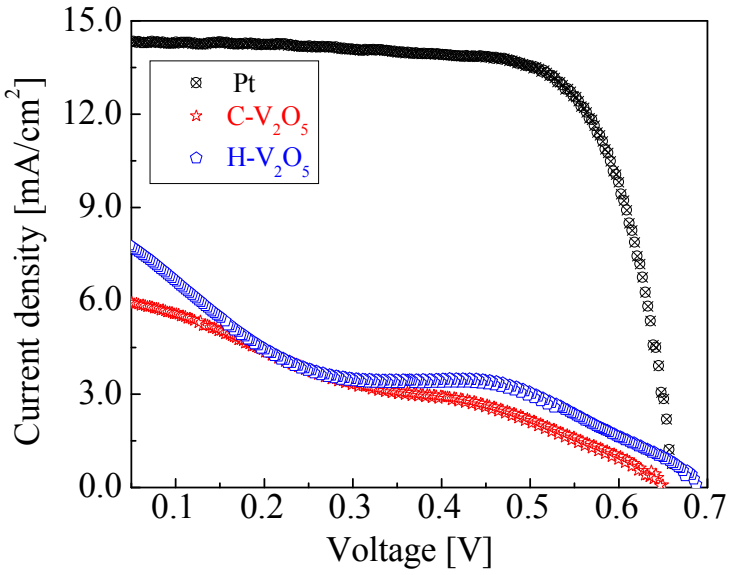

Figure 5. J-V curves of the DSSCs fabricated with C-V_2O_5, H-V_2O_5 and Pt counter electrodes.

Table 1. Photovoltaic parameters of DSSCs using C-V_2O_5, H-V_2O_5 and Pt CE.

Counter Electrode	V_{oc} (V)	J_{sc} (mA-cm^{-2})	FF (%)	η (%)	R_s (Ω-cm^{-2})	R_{sh} (Ω-cm^{-2})
Pt	0.66	14.37	73	6.95	5	1886
C- V_2O_5	0.65	6.36	29	1.2	61	255
H- V_2O_5	0.68	8.34	27	1.6	49	53

3.4. Electrochemical impedance analysis

Electrochemical impedance spectroscopy (EIS) studies were carried out in the dark at the bias 0.9 V to understand the effect of the electrocatalytic activities of different counter electrodes on the I_3^- reduction. The impedance can be described by real (Z^{I}) and imaginary (Z^{II}) components or its modulus ($|Z|$) and the phase shift (φ). The EIS of the electrodes is shown in figure 6. The semicircle in the highest frequency region describes the electron/transport at CE/electrolyte interface [40], which is clearly seen in the case of Pt (inset i) and is not distinctly visible in case

of C-V_2O_5 and H-V_2O_5. The charge transfer resistance across CE/electrolyte (R_{ct}) interface is a crucial parameter on which the power conversion efficiencies of DSSCs rely. The R_{ct} value of the reference electrode Pt is the lowest among all the counter electrodes and H-V_2O_5 is comparatively very much less than that of C-V_2O_5 indicating the higher catalytic activity of Pt than that of the other two counter electrodes. The CV measurements also showed the higher electocatalytic activity of H-V_2O_5 than that of the commercial one. The life time of the electrons was calculated from Bode phase shown in figure 7 using the expression $\tau = 1/2\pi f_{max,}$ where f_{max} is the peak frequency in the mid-frequency region [41]. The life time of the electron for Pt is 11.43 ms, for C-V_2O_5 is 1.59 ms and for H-V_2O_5 is 1.2 ms. The longer electron lifetime for Pt CE based DSSC indicated more effective suppression of the back reaction between the photo-injected electrons and I_3^- in the electrolyte. The CE made of H-V_2O_5 shows better electrocatalytic and photoconversion performances than that of C-V_2O_5. There is a close connection between adhesion of the active material on the substrate and the efficiency of the devices. An improper

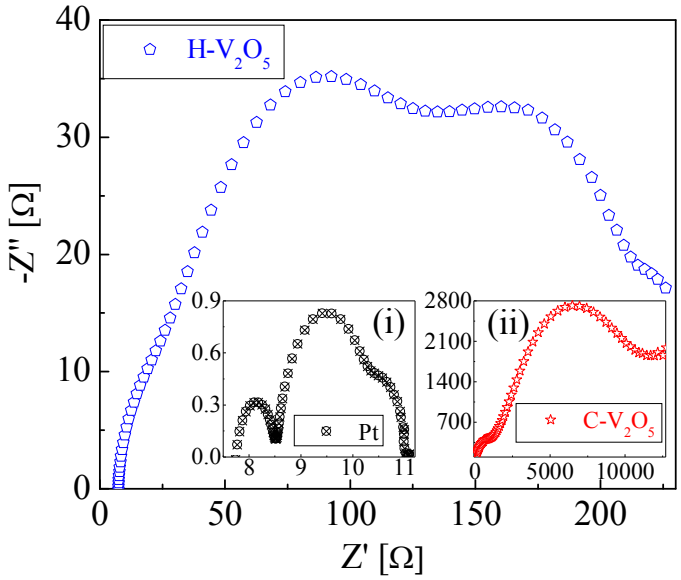

Figure 6. Nyquist plots of devices made of C-V_2O_5, H-V_2O_5 and Pt counter electrodes.

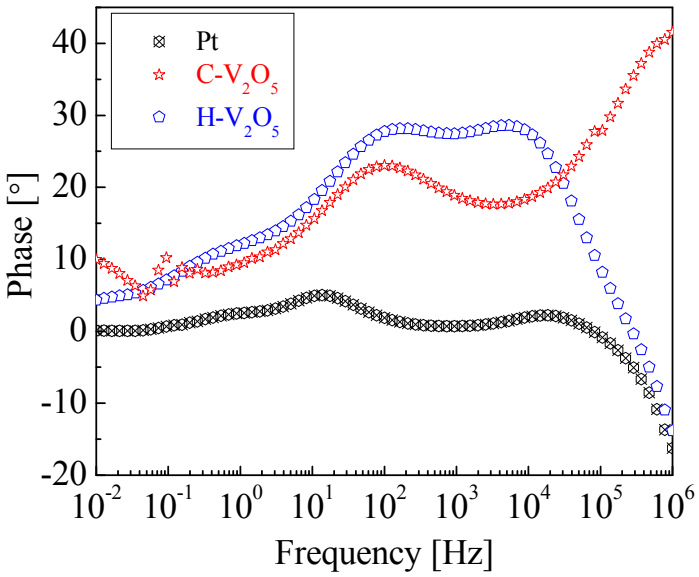

Figure 7. Bode-phase plots of DSSCs made of C-V_2O_5, H-V_2O_5 and Pt counter electrodes.

adhesion of the active material on the FTO substrate affects the photoconversion efficiency [42]. The lower efficiencies of C-V_2O_5 cells are possibly due to improper adhesion which results from the granular features of micron size and the lower surface area of the active material on the FTO substrate. Although the performance of these devices are comparatively low, these results shed light on the possibility of V_2O_5 as a CE, which can significantly reduce the production cost by 5 orders relative to conventional Pt [43]. These results are encouraging as a driver towards more research efforts on V_2O_5 as a CE in the near future. We believe that there is still a plenty of room to further optimize V_2O_5 material in the form of high surface area, tuning the electrical conductivity by doping and its synthesis procedures to fabricate better DSSCs.

4. Conclusion

In summary, for the first time, we have demonstrated the utilization of V_2O_5 as counter electrodes in DSSCs. The C-V_2O_5 and H-V_2O_5 materials were structurally characterized by

powder XRD, which showed the purity of these materials. The surface morphologies of commercial, as-prepared powders, and the screen printed counter electrodes were examined by SEM, which revealed that hydrothermal treatment to C-V_2O_5 has facilitated in reducing the particle size compared to the commercially available ones. Both specimens showed comparable catalytic activity for the tri-iodide reduction. EIS measurements further demonstrated that the electrocatalytic activity of H-V_2O_5 counter electrodes based devices is higher than that of C-V_2O_5. Likewise H-V_2O_5 showed better photovoltaic parameters such as V_{OC}, J_{SC}, and η of 0.68 V, 8.34 mA-cm^{-2} and 1.6% when compared to C-V_2O_5. Since the DSSCs using these counter electrodes still yield low fill factors and low efficiencies as compared to conventional Pt counter electrodes; further improvements need to be carried out. However this looks a promising avenue of investigation since it was found that photovoltaic performance is affected by the morphology of V_2O_5 materials. By tuning the morphology of counter electrodes made of V_2O_5 and improving the layer adhesion, one can likely enhance the device performance and certainly can push the cell efficiencies towards conventional Pt. This work opens a way for further development of more practical and cost effective, stable Pt-free counter electrodes materials for DSSCs.

Acknowledgements

Dr. Jin Xuan and Dr. Jim Buckman of Heriot Watt University are gratefully acknowledged for the access to hydrothermal synthesis and SEM facilities, respectively. We thank EPSRC Supersolar Hub and Council of Scientific and Industrial Research, India (sponsored projects CSC0132 and CSC0122) for financial aid.

References

[1] B. O'Regan, M. Grätzel, A low-cost, high-efficiency solar cell based on dye- sensitized colloidal TiO_2 Films, Nature 353 (1991) 737–740.

[2] M. Gratzel, The advent of macroscopic injection solar cells, Prog. Photovolt. Res. Appl. 14 (2006) 429–442.

[3] A. Yella, H-W. Lee, H. N. Tsao, C. Yi, A. K Chandiran, Md K. Nazeeruddin, E. W-G. Diau, C-Y. Yeh, S. M. Zakeeruddin, M. Grätzel, Porphyrin-sensitized solar cells with cobalt (II/III)–based redox electrolyte exceed 12 percent efficiency, Science 334 (2011) 629-634.

[4] S. Qu, C. Qin, A. Islam, Y. Wu, W. Zhu, J. Hua, H. Tian, L. Han, A novel D–A-p-A organic sensitizer containing a diketopyrrolopyrrole unit with a branched alkyl chain for highly efficient and stable dye-sensitized solar cells, Chem.Commun. 48 (2012) 6972–6974.

[5] E. Olsen, G. Hagen, S. E. Lindquist, Dissolution of platinum in methoxy propionitrile containing LiI/I_2, Sol. Energy Mater. Sol. Cells, 63 (2000) 267-273.

[6] G. Syrrokostas, A. Siokou, G. Leftheriotis, P. Yianoulis, Degradation mechanisms of Pt counter electrodes for dye sensitized solar cells, Sol. Energy Mater. Sol. Cells 103 (2012) 119-127.

[7] S-Q. Fan, B. Fang, J. H. Kim, B. Jeong, C. Kim, J-S. Yu, J. Ko, Ordered multimodal porous carbon as highly efficient counter electrodes in dye-sensitized and quantum-dot solar cells, Langmuir 26 (2010)13644–13649.

[8] H. Wang, K. Sun, F. Tao, D. J. Stacchiola, Y-H. Hu, 3D Honeycomb-like structured graphene and its high efficiency as a counter-electrode catalyst for dye-sensitized solar cells, Angew. Chem. Int. Ed. 125 (2013) 9380–9384.

[9] Z. Yang, M. Liu, C. Zhang, W. W. Tjiu, T. Liu, H. Peng, Carbon nanotubes bridged with graphene nanoribbons and their use in high-efficiency dye-sensitized solar cells, Angew. Chem. Int. Ed. 52 (2013) 3996–3999.

[10] Y. Jo, J-Y. Cheon, J. Yu, H-Y. Jeong, C-H. Han, Y.Jun, S-H. Joo, Highly interconnected ordered mesoporous carbon–carbon nanotube nanocomposites: Pt-free, highly efficient, and durable counter electrodes for dye-sensitized solar cells, Chem. Commun. 48 (2012) 8057–8059.

[11] R. Trevisan, M. Döbbelin, P. P. Boix, E. M. Barea, R. Tena-Zaera, I. Mora- Seró, J. Bisquert, PEDOT nanotube arrays as high performing counter electrodes for dye sensitized solar cells. study of the interactions among electrolytes and counter electrodes, Adv. Energy Mater. 1 (2011) 781–784.

[12] Z. Zhang, X. Zhang, H. Xu, Z. Liu, S. Pang, X. Zhou, S. Dong, X. Chen, G. Cui, $CuInS_2$ Nanocrystals/PEDOT: PSS composite counter electrode for dye-sensitized solar cells

ACS Appl. Mater. Interfaces 4 (2012) 6242–6246.

[13] C. Yuan, S. Guo, S. Wang, L. Liu, W. Chen, E. Wang, Electropolymerization polyoxometalate (pom)-doped pedot film electrodes with mastoid microstructure and its application in dye-sensitized solar cells, Ind. Eng. Chem. Res. 52 (2013) 6694–6703.

[14] R.-Y. Yao, Z-J. Zhou, Z-L. Hou, X. Wang, W-H. Zhou, S-X.Wu, Surfactant-free $CuInS_2$ nanocrystals: an alternative counter-electrode material for dye-sensitized solar cells, ACS Appl. Mater. Interfaces 5 (2013) 3143–3148.

[15] S.-H. Chang, M-D. Lu, Y-L. Tung, H-Y.Tuan, Gram-Scale synthesis of catalytic co_9s_8 nanocrystal ink as a cathode material for spray-deposited, large-area dye-sensitized solar cells, ACS Nano 7 (2013) 9443–9451.

[16] X. Zheng, J. Guo,Y. Shi,F. Xiong,W-H. Zhang, T. Ma, C. Li, Low-cost and high-performance $CoMoS_4$ and $NiMoS_4$ counter electrodes for dye-sensitized solar cells, Chem. Commun. 49 (2013) 9645–9647.

[17] Y. Zhao, A. Thapa,Q. Feng, M. Xi, Q. Qiao, H. Fong, Electrospun TiC/C nano-felt surface-decorated with Pt nanoparticles as highly efficient and cost-effective counter electrode for dye-sensitized solar cells, Nanoscale 5 (2013) 11742–11747.

[18] Z. Wen, S. Cui , H. Pu , S. Mao , K. Yu , X. Feng ,J. Chen, Metal nitride/graphene nanohybrids: general synthesis and multifunctional titanium nitride/graphene electrocatalyst, Adv. Mater. 23 (2011) 5445–5450.

[19] W. Wei, H. Wang, Y-H. Hu, Unusual particle-size-induced promoter-to-poison transition of ZrN in counter electrodes for dye-sensitized solar cells,J. Mater. Chem. A 1 (2013) 14350–14357.

[20] M.-S. Wu, J.-F.Wu, Pulse-reverse electrodeposition of transparent nickel phosphide film with porous nanospheres as a cost-effective counter electrode for dye-sensitized solar cells, Chem. Commun. 49 (2013) 10971–10973.

[21] J.Guo, Y. Shi, Y. Chu, T. Ma, Highly efficient telluride electrocatalysts for use as Pt-free counter electrodes in dye-sensitized solar cells, Chem. Commun. 49 (2013) 10157–10159.

[22] R. Bajpai, S. Roy, P. Kumar, P. Bajpai, N. Kulshrestha, J. Rafiee, N. Koratkar, D. S. Misra, Graphene supported platinum nanoparticle counter-electrode for enhanced performance of dye-sensitized solar cells, ACS Appl. Mater. Interfaces 3 (2011) 3884–3889.

[23] V.-D. Dao, L. L. Larina, K-D. Jung, J-K. Lee and H-S. Choi, Graphene–NiO nanohybrid prepared by dry plasma reduction as a low-cost counter electrode material for dye-sensitized solar cells, Nanoscale 6 (2014) 477–482.

[24] P. Sudhagar, S. Nagarajan, Y-G.Lee, D. Song, T. Son, W. Cho, M. Heo, K.Lee, J. Won, Y-S. Kang,

Synergistic catalytic effect of a composite (CoS/PEDOT:PSS) counter electrode on triiodide reduction in dye-sensitized solar cells, ACS Appl.Mater. Interfaces 3 (2011) 1838–1843.

[25] M.Wu, X. Lin, Y. Wang, L. Wang, W. Guo, D. Qi, X. Peng, A. Hagfeldt, M. Grätzel, T. Ma, Economical Pt-free catalysts for counter electrodes of dye sensitized solar cells J. Am. Chem. Soc.134 (2012) 3419−3428.

[26] M. Wu, X. Lin, A. Hagfeldt, T. Ma, A novel catalyst of WO_2 nanorod for the counter electrode of dye-sensitized solar cells, Chem. Commun. 47 (2011) 4535–4537.

[27] L. Cheng, Y. Hou, B. Zhang, S. Yang, J-W. Guo, L. Wua, H-G Yang, Hydrogen-treated commercial WO_3 as an efficient electrocatalyst for triiodide reduction in dye-sensitized solar cells, Chem. Commun.49 *(*2013) 5945-5957.

[28] C. Julien, B. Yebka, J. P. Guesdon, Solid-state lithium microbatteries, Ionics 1 (1995) 316-327.

[29] R. M. Wightman, Voltammetry with microscopic electrodes in new domains, Science 240 (1988) 415-420.

[30] L. Krusin-Elbaum, D. M. Newns, H. Zeng, V. Derycke , J. Z. Sun, R. Sandstrom, Room-temperature ferromagnetic nanotubes controlled by electron or hole doping, Nature431 (2004) 672-676.

[31] C. M. Leroy, M-F. Achard, O. Babot, N. Steunou, P. Massé, J. Livage, L .Binet, Nicolas Brun, R. Backov, Designing nanotextured vanadium oxide-based macroscopic fibers: application as alcoholic sensors,Chem. Mater.19 (2007) 3988-3999.

[32] G. Rizzo, A. Arena, A. Bonavita, N. Donato, G. Neri, G. Saitta, Gasochromic response of nanocrystalline vanadium pentoxide films deposited from ethanol dispersions, Thin Solid Films 518 (2010) 7124-7127.

[33] Y. Fujita, K. Miyazaki, T. Tatsuyama, On the electrochromism of evaporated V_2O_5 films, Jpn. J. Appl. Phys. 24 (1985) 1082-1086.

[34] H. Elbohy, A. Thapa, P.Poudel, N. Adhikary, S. Venkatesan, Q.Qiao, Vanadium oxide as new charge recombination blocking layer for high efficiency dye-sensitized solar cells, Nano Energy 13 (2015) 368–375.

[35] M. Kovendhan,D. P. Joseph, P. Manimuthu, A. Sendilkumar , S.N. Karthick , S. Sambasivam , K. Vijayarangamuthu, H. J. Kim , Byung Chun Choi , K. Asokan , C. Venkateswaran , R. Mohan, Prototype electrochromic device and dye sensitized solar cell using spray deposited undoped and 'Li' doped V2O5 thin film electrodes, Current Applied Physics 15 (2015) 622-631.

[36] M. Sethupathy, S. Ravichandran, P. Manisankar, Preparation of PVdF-PAN-V2O5 hybrid composite membrane by electrospinning and fabrication of dye-sensitized solar cells, Int. J.

Electrochem.Sci. 9 (2014) 3166 – 3180.

[37] J. Xia, C.Yuan, S.Yanagida, Novel counter electrode V_2O_5/Al for solid dye-sensitized solar cells, ACS Appl. Mater. Interfaces 2 (2010) 2136–2139.

[38] J. Rodríguez-carvajal, Recent advances in magnetic structure determination by neutron powder diffraction, Physica B 192 (1993) 55-69.

[39] J. Tauc, Amorphous and liquid semiconductors, first ed., Plenum Press, New York, 1974.

[40] F.F. Santiago, J. Bisquert, E. Palomares, L. Otero, D. Kuang, S.M. Zakeeruddin, M.Grätzel, Correlation between photovoltaic performance and impedance spectroscopy of dye-sensitized solar cells based on ionic liquids, J. Phys. Chem. C 111 (2007) 6550–6560.

[41] N.G. Park, M.G. Kang, K.M. Kim, K.S. Ryu, S.H. Chang, D.K. Kim, J.V.D. Lagemaat, K.D. Benkstein, A.J. Frank, Morphological and photoelectrochemical characterization of core−shell nanoparticle films for dye-sensitized solar cells: Zn−O type shell on SnO_2 and TiO_2 cores , Langmuir 47 (2004) 4246–4253.

[42] H-J. Kim, C-W. Kim, D. Punnoose, C.V.V.M.Gopi, S-K. Kim, K. Prabakar, S. S. Rao, Nickel doped cobalt sulfide as a high performance counter electrode for dye-sensitized solar cells, Applied Surface Science 328 (2015) 78–85.

[43] http://www.sigmaaldrich.com/chemistry/aldrich-chemistry/aldrich-handbook.html.